Pergamon

Acta mater. Vol. 47, No. 1, pp. 247–257, 1999

Printed in Great Britain
PII: S1359-6454(98)00323-1
1359-6454/99 $19.00 + 0.00

SHAPE EVOLUTION AND SPLITTING OF COHERENT PARTICLES UNDER APPLIED STRESSES

D. Y. LI†‡ and L. Q. CHEN

Department of Materials Science and Engineering, The Pennsylvania State University, University Park, PA 16802, U.S.A.

(Received 30 December 1997; accepted 29 August 1998)

Abstract—Morphological evolution and splitting of coherent precipitate particles under applied stresses were investigated using a diffuse-interface field kinetic approach. A particular example, γ' precipitates in Ni-based superalloys, was studied. In the absence of externally applied stress, a coherent γ' particle exhibits a cuboidal shape, as a result of the competition between anisotropic coherency strain energy and nearly isotropic specific interfacial energy. It was demonstrated that under a uniaxial applied constraint strain, growth of the γ' particle became tetragonal, resulting in a shape transformation from being cuboidal to tetragonal. As the magnitude of the applied strain was further increased, it is interesting to observe that the γ' particle became unstable and split into two or more parallel plates. The influences of stress magnitude, precipitate volume fraction, and interfacial energy on the splitting process are discussed. © *1998 Acta Metallurgica Inc. Published by Elsevier Science Ltd. All rights reserved.*

1. INTRODUCTION

Solid-state phase transformations, very often, produce second-phase precipitate particles coherently embedded in the parent phase matrix, followed by particle coarsening during which large particles grow at the expense of smaller ones. Morphology of the precipitate particles, i.e. the sizes, shapes, volume fraction, crystallographic relations with the matrix, and the mutual arrangement of the particles, plays an important role in determining mechanical, electric and magnetic properties of the material.

Thermodynamically, in the absence of applied stress, the morphology of a single coherent particle is determined by two factors: (1) the interfacial energy between the precipitate and the matrix, and (2) the coherency elastic strain energy arising from the lattice accommodation across the coherent interface. The interfacial energy of a coherent particle is roughly proportional to its interfacial area, and the interfacial energy affects the morphology through its orientational dependence. On the other hand, the elastic strain energy of a coherent particle is roughly proportional to its volume, and the elastic strain energy depends on the morphology through its dependence on the elastic anisotropy and the crystallographic relation between the precipitate and the matrix.

The morphology of a coherent particle can, in general, be changed by applied stresses. Roughly speaking, an applied stress has two effects. One effect is that the applied stress can cause an additional lattice mismatch strain, $\Delta\varepsilon$, when elastic constants of the precipitate and the matrix are different

$$\Delta\varepsilon \sim \frac{\Delta\lambda}{\bar{\lambda}^2}\sigma^{\mathrm{a}} \tag{1}$$

where $\Delta\lambda$ is the modulus difference between the precipitate and the matrix, $\bar{\lambda}$ the average modulus of the two-phase solid, and σ^{a} the magnitude of the applied stress. The second effect is a coupling potential energy caused by the applied stress

$$F_{\mathrm{coup}} = -\int_V \bar{\varepsilon}\sigma^{\mathrm{a}}\,\mathrm{d}^3\vec{r} \approx -V\sum_p \omega_p \varepsilon(p)\sigma^{\mathrm{a}} \tag{2}$$

where $\bar{\varepsilon}$ is the homogeneous strain, and ω_p the volume fraction of p-type of precipitates with transformation strain $\varepsilon(p)$.

If a system is homogeneous in terms of its elastic modulus, i.e. $\Delta\lambda = 0$, the contribution from an applied stress to the total driving force for morphological evolution is given only by the coupling term. In this case, an applied stress affects only the volume fractions of different types of precipitates but not their shapes. For a particular example, a γ' precipitate in a γ matrix, both γ and γ' phases are cubic (i.e. the lattice misfit is dilatational). If ignoring the difference in elastic modulus between the γ' and γ phases, one may find that the coupling term only affects the volume fraction of the γ' phase. However, when a solid is elastically inhomogeneous,

†Present address: Department of Chemical and Materials Engineering, University of Alberta, Edmonton, Alberta, Canada T6G 2G6.

‡To whom all correspondence should be addressed.

i.e. each phase has a different elastic modulus, an applied stress will produce different elastic deformation within each phase. As a result, this stress field will cause an extra lattice mismatch in addition to the lattice mismatch that is caused by the stress-free lattice parameter difference, thus resulting in a variation in morphology. Therefore, in order to study the effect of applied stress on the morphological evolution of γ' particles, the difference in elastic modulus between γ' and γ matrix must be taken into account.

There have been a number of analytical studies on relative stabilities of different shapes of a coherent particle under the influence of coherency strain energy but in the absence of applied stress [1–5], and on the temporal evolution during growth or coarsening by numerical simulations [6–16]. It is generally agreed that the interfacial energy anisotropy is small at relatively high temperatures at which particle growth and coarsening occur. Therefore, for a cubic precipitate in a cubic matrix, when the precipitate size is small or if the lattice mismatch is negligible, the shape of a particle is spherical or nearly spherical. As the particle size increases, the elastic energy becomes increasingly important, and the shape will gradually become cuboidal. One of the most intriguing phenomena during shape evolution is the possibility of particle splitting as observed experimentally in Ni-based superalloys [17–22]. The theoretical analysis by Khachaturyan *et al.* [4] showed that there is a critical size beyond which an eight-particle split configuration, or octet, has a lower energy than a single cuboidal particle. Lee [13] developed a discrete atom method and applied it to modeling morphological evolution of coherent precipitates. He demonstrated that with a decrease in interfacial energy, the coherency elastic energy becomes predominant and a coherent particle is easier to split or to be branched. Numerical simulations by McCormack *et al.* [7] based on a finite-element Monte-Carlo approach and by Wang *et al.* [6] using microscopic diffusion equations also demonstrated that a single overgrown particle can indeed split into two particles, or a doublet. Most recently, employing the continuum diffuse-interface field model, Zhang *et al.* [23] showed that a single coherent particle may split into four particles in two dimensions and eight particles in three dimensions. By including thermal noise in the model, they demonstrated that other split particle configurations are possible, such as two- and three-particle configurations in two dimensions.

Since the instability of a γ' coherent particle with respect to splitting is caused by the internal misfit strain between the γ' phase and the γ matrix, similar instabilities should be expected in the presence of applied stresses or strains. Since the magnitude of additional elastic strain produced by an applied stress is proportional to the magnitude of the applied stress, one would expect to observe the splitting instability of an initially stable single coherent particle during its evolution to equilibrium state under high applied stresses. Therefore, the main objective of this research is to investigate the morphological evolution of a coherent particle under an externally applied stress using a diffuse-interface field approach. Previously we investigated the γ' precipitate growth and rafting of the γ' phase in Ni-based superalloys under applied constant strains [24]. In this paper, we focus on exploring the possibility of particle splitting in the presence of externally applied stress. In particular, effects of the magnitude of the applied stress, the precipitate volume fraction and the interfacial energy on the particle splitting process are discussed.

2. THE DIFFUSE-INTERFACE FIELD MODEL

A diffuse-interface phase-field model was employed for the simulation study. This approach was described in detail in a number of papers [6, 11, 24–27]. The specific application of this model to microstructural evolution of γ' precipitates in Ni-based superalloys was reported in Refs [24, 28]. In order to make this paper self-contained, a brief description of the model is presented. In this diffuse-interface model, the microstructure of a ($\gamma' + \gamma$) two-phase mixture is described by both a composition field variable, $C(\vec{r},t)$, and structural order parameter field variables, $\eta_i(\vec{r},t)$. The composition and the structural order parameter variables, respectively, distinguish compositional and structural differences between the γ' phase and the γ matrix. The γ' phase has an ordered f.c.c. lattice structure, transforming from the disordered f.c.c. γ matrix. An ordered f.c.c. crystal has four equivalent ordered states, obtained by displacements of the crystal lattice from its origin to [0,0,0], $[\frac{1}{2},\frac{1}{2},0]$, $[\frac{1}{2},0,\frac{1}{2}]$, and $[0,\frac{1}{2},\frac{1}{2}]$, respectively [29]. Four types of γ' domains may therefore exist in the γ matrix, whose ordering states can be described using three order parameters η_i ($i = 1,2,3$) with four different combinations [24, 29]. The four combinations of the order parameters are $(1,1,1)\eta$, $(\bar{1},\bar{1},1)\eta$, $(\bar{1},1,\bar{1})\eta$, and $(1,\bar{1},\bar{1})\eta$, respectively, corresponding to the four γ' domains. When the order parameter η is equal to its equilibrium value η_0, the γ' domains reach their equilibrium states. Microstructural development is described by temporal evolution of the $C(\vec{r},t)$ and $\eta_i(\vec{r},t)$ field variables; and graphically, a microstructure may be represented by either the composition field, $C(\vec{r},t)$, or the order parameter fields, $\sum_i \eta_i^2(\vec{r},t)$.

The growth of γ' precipitates proceeds with a decrease in the system free energy, which includes the incoherent free energy, the interphase boundary energy and the coherency elastic energy. The chemical energy density may be approximated using a Landau free energy polynomial

$$f(C,\eta_i) = \frac{A_1}{2}(C - C_1)^2 + \frac{A_2}{2}(C - C_2)\sum_i^3 \eta_i^2 - \frac{A_3}{3}\eta_1\eta_2\eta_3 + \frac{A_4}{4}\sum_i^3 \eta_i^4 + \frac{A_5}{4}\left(\sum_i^3 \eta_i^2\right)^2 \quad (3)$$

where A_1, A_2, A_3, A_4, and A_5 are coefficients whose values were chosen, respectively, as 40.0, 17.0, 46.8, 15.0, and 5.0 (with a unit: [u] = 10^8 erg/cm^3). Values of C_1 and C_2 are 0.05 and 0.22, respectively. The choice of these values provides equilibrium compositions at $C_\gamma = 0.054$ for the Ni–Al (γ) matrix and $C_{\gamma'} = 0.242$ for the γ' precipitates. By minimizing $f(C,\eta_i)$ with respect to the order parameter at a given C for a single γ' variant [e.g. described by (1,1,1)η], one may obtain the relationship between C and the equilibrium order parameter $\eta = \eta_0$. Therefore, $f(C,\eta)$ can be expressed as a function of the composition only, i.e. $f(C,\eta_0) = f(C,\eta_0(C))$ as Fig. 1 illustrates. This function has two branches. One was obtained at $\eta = 0$, corresponding to the matrix phase. The other was obtained at $\eta = \eta_0$ corresponding to the γ' phase. In order to investigate the splitting of the γ' phase, one only needs to investigate one single γ' particle [e.g. the (111)η variant]. Therefore, equation (3) can be simplified to the following form:

$$f(C,\eta) = \frac{A_1}{2}(C - C_1)^2 + \frac{3A_2}{2}(C_2 - C)\eta^2 - \frac{A_3}{3}\eta^3 + \frac{3A_4 + 9A_5}{4}\eta^4. \quad (4)$$

The total incoherent free energy in the diffuse-interface field model is given by

$$F_{\text{inc}} = \int_V \left[f(C/(\vec{r},t),\eta(\vec{r},t)) + \frac{3\alpha}{2}(\nabla\eta(\vec{r},t))^2 + \frac{\beta}{2}(\nabla C(\vec{r},t))^2 \right] \mathrm{d}^3\vec{r} \quad (5)$$

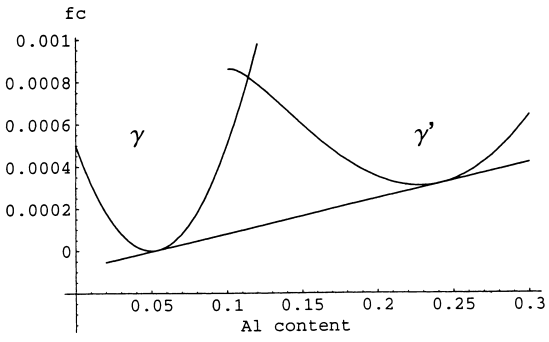

Fig. 1. Specific chemical-free energies of γ' and γ phases vs composition, calculated using equation (4).

where the gradient terms represent the contribution from the interphase boundary energy, and α and β are gradient coefficients. In this work, isotropic interphase boundary energy is assumed.

An important contribution to the system's total free energy is the coherency elastic energy caused by the lattice mismatch between the γ' precipitates and the matrix. The coherency strain energy has been extensively studied [30–42]. In general, for an elastically inhomogeneous system, the elastic strain energy has to be computed numerically for a given microstructure. However, for systems with small inhomogeneity, as shown by Khachaturyan *et al.* [42], the problem can be solved analytically using the effective medium approximation. The elastic energy in terms of the inhomogeneous composition field variable with diffusive interphase boundary is given as (see the Appendix A)

$$E_{\text{el}} = \frac{V}{2}\bar{\lambda}_{ijkl}\bar{\varepsilon}_{ij}\bar{\varepsilon}_{kl} - V\Delta\lambda_{ijkl}\bar{\varepsilon}_{ij}\overset{\circ}{\varepsilon}_{kl}\overline{(\Delta C)^2} + \frac{V}{2}\bar{\lambda}_{ijkl}\overset{\circ}{\varepsilon}_{ij}\overset{\circ}{\varepsilon}_{kl}\overline{(\Delta C)^2} - \frac{1}{2}\int\frac{\mathrm{d}^3\vec{q}}{(2\pi)^3}[n_k\sigma^*_{ki}\Omega(\vec{n})_{ij}\sigma^*_{jl}n_l]|\tilde{C}(\vec{q})|^2 \quad (6)$$

where $\bar{\lambda}_{ijkl} = \lambda^*_{ijkl}\langle C(\vec{r})\rangle + \lambda_{ijkl}(1 - \langle C(\vec{r})\rangle)$ is the average elastic modulus; λ^*_{ijkl} and λ_{ijkl} are, respectively, the elastic moduli of the γ' precipitates and the matrix. V is the total volume of the system. $\sigma^*_{ij} = \bar{\lambda}_{ijkl}\overset{\circ}{\varepsilon}_{kl} - \Delta\lambda_{ijkl}\bar{\varepsilon}_{kl}$ is the effective eigenstress, where $\Delta\lambda_{ijkl} = \lambda^*_{ijkl} - \lambda_{ijkl}$. $\vec{q}$ and $\vec{n} = \vec{q}/q$ are, respectively, a vector and corresponding unit vector in the reciprocal space. $\Omega(\vec{n})_{ij}$ is a Green function reciprocal to $\Omega^{-1}(\vec{n})_{ij} = n_l\bar{\lambda}_{lijm}n_m$. $\tilde{C}(\vec{q})$ is the Fourier transform of the variation of the composition field variable, i.e. $\Delta C(\vec{r}) = C(\vec{r}) - \bar{C}$. $\bar{\varepsilon}_{ij}$ is the homogeneous strain which determines the macroscopic shape deformation caused by internal and external stresses.

When the system is under a constant applied strain (i.e. under a constraint strain with fixed boundary), the homogeneous strain is the applied strain, i.e. $\bar{\varepsilon}_{ij} = \bar{\varepsilon}^{\text{a}}_{ij}$. Equation (6) thus becomes

$$E^{\varepsilon}_{\text{el}} = \frac{V}{2}\bar{\lambda}_{ijkl}\bar{\varepsilon}^{\text{a}}_{ij}\bar{\varepsilon}^{\text{a}}_{kl} - V\Delta\lambda_{ijkl}\bar{\varepsilon}^{\text{a}}_{ij}\overset{\circ}{\varepsilon}_{kl}\overline{(\Delta C)^2} + \frac{V}{2}\bar{\lambda}_{ijkl}\overset{\circ}{\varepsilon}_{ij}\overset{\circ}{\varepsilon}_{kl}\overline{(\Delta C)^2} - \frac{1}{2}\int\frac{\mathrm{d}^3\vec{q}}{(2\pi)^3}[n_k\sigma^*_{ki}\Omega(\vec{n})_{ij}\sigma^*_{jl}n_l]|\tilde{C}(\vec{q})|^2. \quad (7)$$

If the system is under a constant applied stress, the elastic potential should include the external work, that is

$$E_{\mathrm{el}}^{\sigma} = \frac{V}{2}\bar{\lambda}_{ijkl}\bar{\varepsilon}_{ij}\bar{\varepsilon} - V\Delta/\lambda_{ijkl}\bar{\varepsilon}_{ij}\overset{\circ}{\varepsilon}_{kl}\overline{(\Delta C)^2} + \frac{V}{2}\bar{\lambda}_{ijkl}\overset{\circ}{\varepsilon}_{ij}\overset{\circ}{\varepsilon}_{kl}\overline{(\Delta C)^2} - \frac{1}{2}\int\frac{\mathrm{d}^3\vec{q}}{(2\pi)^3}[n_k\sigma_{kl}^{*}\Omega(\vec{n})_{ij}\sigma_{jl}^{*}n_l]|\tilde{C}(\vec{q})|^2 - \int_V \sigma_{ij}^{\mathrm{a}}\bar{\varepsilon}_{ij}\,\mathrm{d}^3\vec{r} \quad (8)$$

where

$$\bar{\varepsilon}_{op} \approx \left(\bar{S}_{opij}\Delta\lambda_{ijsq}\overset{\circ}{\varepsilon}_{sq}\overline{(\Delta C)^2} - \frac{\Delta\lambda_{oplm}A_{lmsq}}{V}\right)\overset{\circ}{\varepsilon}_{sq} + \bar{S}_{opij}\sigma_{ij}^{\mathrm{a}}$$

and

$$\sigma_{ij}^{\mathrm{a}} = \bar{\lambda}_{ijkl}\bar{\varepsilon}_{kl} - \bar{\lambda}_{ijkl}\overset{\circ}{\varepsilon}_{kl}\overline{(\Delta C)^2} + \frac{1}{V}\Delta\lambda_{ijkl}A_{klmn}(\bar{\lambda}_{mnop}\overset{\circ}{\varepsilon}_{op} - \Delta\lambda_{mnop}\bar{\varepsilon}_{op})$$

with

$$A_{klmn} = -\int\frac{\mathrm{d}^3\vec{q}}{(2\pi)^3}n_k\Omega(\vec{n})_{lm}n_n|\tilde{C}(\vec{q})|^2.$$

For the present study, the simulation of the growth and splitting of the γ' phase under applied stresses was performed under the strain constraint condition.

The morphological evolution is determined by solving the non-linear differential kinetic equations for the field variables. The composition field is determined by solving the Cahn–Hilliard diffusion equation [43], whereas the order parameter field variable is determined by solving the Ginzburg–Landau equation [44]

$$\frac{\mathrm{d}C(\vec{r},t)}{\mathrm{d}t} = M\nabla^2\frac{\delta F}{\delta C(\vec{r},t)},\quad \frac{\mathrm{d}\eta}{\mathrm{d}t} = -L\frac{\delta F}{\delta\eta(\vec{r},t)} \quad (9)$$

where M and L are kinetic coefficients which characterize the atomic diffusivity and interphase boundary mobility. Under the strain constraint condition, the system is connected to a thermal reservoir but mechanically isolated (i.e. no external work). In this case, $F = F_{\mathrm{inc}} + E_{\mathrm{el}}^{\varepsilon}$ is the Helmholtz free energy of the system. If the system is subjected to a constant applied stress, the system is connected to a mechanical reservoir as well as to a thermal reservoir. The free energy of such a system is the Gibbs free energy, i.e. $F = F_{\mathrm{inc}} + E_{\mathrm{el}}^{\sigma}$. These differential kinetic equations were solved numerically in the reciprocal space.

3. RESULTS AND DISCUSSION

The simulation was conducted in two-simulational space. The kinetic equations were discretized using a 256×256 square grid with the unit length of the grid equal to l. The value of l was not artificially fixed, but determined by fitting interfacial energy in the following way. We chose the gradient coefficients, α and β, in equation (5) equal to 0.4 ($\times 10^8$ erg/cm). The corresponding interfacial energy can be calculated by setting up a flat boundary separating the γ' precipitate phase and the γ matrix phase. For the particular parameters used in this simulation, the calculated specific interfacial energy is equal to $1.25(\times 10^8\ \mathrm{erg/cm^3})\Delta x$, where Δx is the spatial discretization grid length. By fitting this calculated energy to available data of γ'/γ interfacial energy, $\sigma_{\mathrm{s}} = 24.3\ \mathrm{erg/cm^2}$, given by Hirata and Kirkwood [45], we determined the grid length Δx which is equal to 19.4 Å ($= l$) in real unit. In this simulation, we used a reduced unit, $\Delta x^{*} = \Delta x/l = 1.0$, for the grid size.

Reduced time was used in the simulation: $t^{*} = n \cdot \tau$, where n is the iteration time step for the numerical integration of the kinetic equations, and τ the time step for each iteration which is chosen to be 0.01. To relate this reduced time to real time unit, we fitted the coefficient M to the chemical diffusion coefficient in the disordered phase. If we assume that the composition in the disordered matrix is uniform, the diffusion equation becomes

$$\frac{\partial C}{\partial t} = M\nabla^2\frac{\delta F}{\delta C} = \left(M\frac{\partial^2 f}{\partial C^2}\right)\nabla^2 C = D\nabla^2 C \quad (10)$$

where D is the chemical diffusion coefficient in the disordered phase and f the local free energy density. Using equation (4) for the free energy density, in the disordered state, we may obtain the relationship between M and D

$$D = M\left.\frac{\partial^2 f}{\partial C^2}\right|_{\eta_i=0} = MA_1. \quad (11)$$

The Cahn–Hilliard equation expressed using the chemical diffusion coefficient is thus given by

$$\frac{\partial C}{\partial t} = \frac{D}{A_1}\nabla^2\frac{\delta F}{\delta C}. \quad (12)$$

In reduced units

$$\frac{\partial C}{\partial t^{*}} = \nabla^{*2}\frac{\delta F}{\delta C} \quad (13)$$

where $t^{*} = t(D/A_1 l^2)$ and $\nabla^{*2} = l^2\nabla^2$. Both F and A_1 are in reduced units which are related to the real unit by multiplying by $10^8\ \mathrm{erg/cm^3}$. The kinetic equation for the order parameters is also in reduced units and we set $LA_1 l^2/D = 1.0$ in the simulation (please note that A_1 here is unitless). According to Hirata and Kirkwood [45], the diffusion coefficient D of Ni–Al alloy at 695°C is $6.51 \times 10^{-15}\ \mathrm{cm^2/s}$. This value of D was used in our simulation to determine the real evolution time $t = t^{*}/(D/A_1 l^2)$.

In order to investigate the growth of a γ' particle under an applied constant strain, a uniaxial stress was initially applied to the system, followed by fixing the body boundary to generate a constant constraint strain field. Elastic constants of the γ' phase

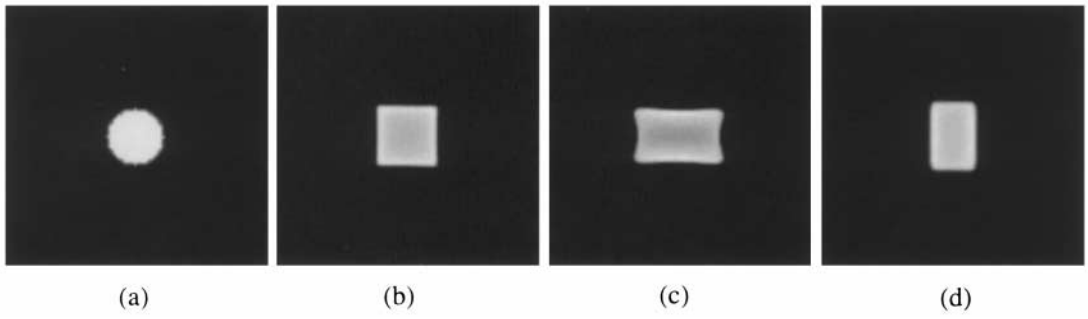

Fig. 2. Morphologies of a γ' particle grown in a supersaturated γ matrix with $c_m = 0.08$ ($t = 1.62$ h): (a) the initially embedded γ' particle; (b) grown without external strain constraint; (c) grown under a tensile stress (40 MPa) applied horizontally; (d) grown under a compressive strain (40 MPa) applied horizontally.

and the NiAl (γ) matrix (in units of 10^{11} erg/cm^3) are $C^*_{11} = 1.67$, $C^*_{12} = 1.07$, $C^*_{44} = 0.99$, $C_{11} = 1.12$, $C_{12} = 0.63$, and $C_{44} = 0.57$, respectively [18]. The eigenstrain of γ' is dilatational and expressed as $\overset{\circ}{\varepsilon}_{ij} = \varepsilon_0 \delta_{ij}$, where $\varepsilon_0 = 0.563\%$ [18].

3.1. Morphological evolution of a γ' particle in the absence of external constraint strain

The main objective of the research is to investigate the growth behavior of the γ' phase under applied stresses in the constraint strain boundary condition. For comparison, morphological evolution of a γ' particle in the absence of a constraint strain was first simulated. At the beginning of the simulation, a circular γ' particle with radius equal to $30\Delta x^*$ was initially embedded in the matrix. Figure 2(b) illustrates the morphology of a γ' particle evolved from the initially embedded γ' particle [see Fig. 2(a)] in a supersaturated NiAl matrix with $c_m = 0.08$ and $\eta = 0$. It was demonstrated that the grown γ' particle changed its circular shape to a square (cuboidal in three dimensions), with its $\{100\}_{\gamma'}$ plane parallel to the $\{100\}_{\gamma}$ plane of the matrix. Since the γ'/γ interphase boundary energy was assumed to be isotropic, the cuboidal shape and the $(100)_{\gamma'} \| (100)_{\gamma}$ orientation relationship are therefore attributable to the anisotropy of the elastic interactions. The simulated morphology of γ' particles is consistent with experimental observations [18, 20, 46]. The cuboidal shape of the γ' particle has been theoretically analyzed by a number of researchers [8, 13, 47–52].

3.2. Tetragonal growth under applied constraint strains

The cuboidal shape transformation was changed when a constraint strain was applied to the system. Figure 2(c) illustrates the morphology of a γ' particle developed under a tensile strain $\bar{\varepsilon}^a_{ij}$, applied along the x-axis (i.e. the horizontal direction). The strain was introduced by a tensile stress equal to $0.004(\times 10^{11}\ \text{erg/cm}^3) = 40$ MPa which was applied before the system's boundary was fixed. It is demonstrated that the γ' particle was elongated along the applied tensile strain. This tetragonal growth may be explained from the effective eigenstrain, $\varepsilon^*_{ij} = \bar{S}_{ijpq}\sigma^*_{pq} = \overset{\circ}{\varepsilon}_{ij} - \Delta\varepsilon^a_{ij}$, where $\Delta\varepsilon^a_{ij} = \bar{S}_{ijpq}\Delta\lambda_{pqkl}\bar{\varepsilon}^a_{kl}$ and $\bar{S}_{ijpq}$ is the average elastic compliance. The effective eigenstrain corresponds to the effective stress σ^*_{pq} in equation (6). In the absence of the applied strain, the eigenstrain is a pure dilatational strain, i.e. $\overset{\circ}{\varepsilon}_{ij} = \varepsilon_0 \delta_{ij}$, which causes a cuboidal morphology of the γ' phase. When a strain is applied along the x-axis, it results in $\Delta\varepsilon^a_{xx} > \Delta\varepsilon^a_{yy}$ because of the positive $\Delta\lambda_{pqkl}$, thus leading to $\varepsilon^*_{xx} < \varepsilon^*_{yy}$. As a result, the tetragonal growth of the γ' phase occurs with its elongation along the x-axis. A compressive strain, however, makes the elongation along the y-axis perpendicular to the applied strain [see Fig. 2(d)], since in this case, $\varepsilon^*_{xx} > \varepsilon^*_{yy}$. It is

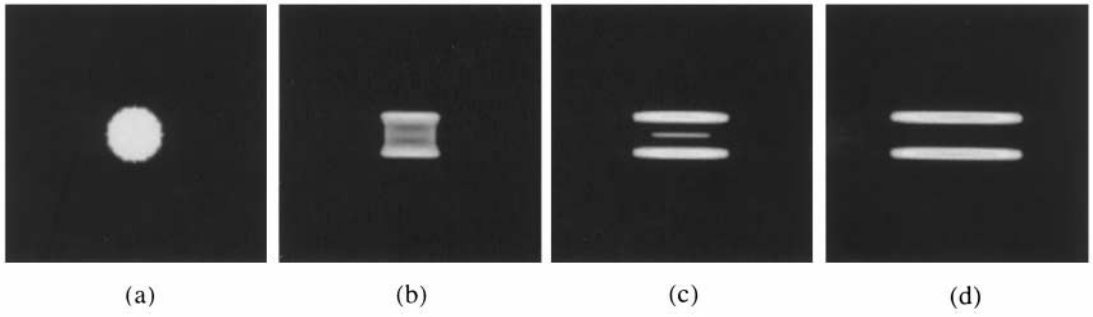

Fig. 3. Splitting of a γ' particle in a γ matrix with $c_m = 0.08$ under a tensile stress $\sigma = 80$ MPa applied along the horizontal direction: (a) $t = 0$; (b) $t = 0.18$ h; (c) $t = 0.54$ h; (d) $t = 1.62$ h.

noted that the elongation direction is also influenced by the sign of $\Delta\lambda_{pqkl}$. Under a tensile stress, a soft precipitate ($\Delta\lambda_{pqkl}<0$) is elongated along the direction perpendicular to the applied stress, while a hard precipitate ($\Delta\lambda_{pqkl} > 0$) is elongated along the applied stress. Besides, the sign of the lattice mismatch ε_0 also influences the elongation direction [1, 18, 53–55]. The final elongation direction can be readily predicted by analyzing the effective eigenstrain. These analyses well explain experimental observations. The tetragonal growth of the γ' phase under external applied stress was also computationally demonstrated by a number of researchers such as Laberge *et al*. [56], Gayda and Srolovitz [57], and Valles and Arrell [58] using Monte Carlo approaches, and Nishimori and Onuki [59] using a dynamic model.

3.3. Splitting of γ' particles under applied constraint strains

The tetragonal growth of γ' was further changed by increasing the magnitude of the applied strain. Our simulation demonstrates that a γ' particle may split into a doublet of parallel plates under higher applied constraint strains. Figure 3 illustrates the growth of the γ' particle under an applied tensile strain which is two times higher than that causing tetragonal growth as shown in Fig. 2(c). As observed, under the higher applied strain the tetragonal growth was speeded up and the particle split away and eventually changed to a doublet of two parallel plates. It is believed that this splitting of the γ' particle is caused by the stress relaxation, associated with a decrease in the total free energy of the system. Wang and Khachaturyan [52], Lee [13], and Zhang *et al*. [23] explained the morphological instability of γ' particles under the influence of coherency elastic strain and discussed the particle splitting based on the competition between the coherency elastic energy and the interfacial energy. Their explanations are also applicable to the case of the splitting under an external load which modifies the lattice mismatch as equation (1) indicates. However, as observed, an applied load can affect the splitting direction, e.g. a particle may split into a doublet of two plates parallel to a tensile strain or perpendicular to a compressive strain applied in the [100] direction. In addition, it is interesting to observe that the splitting process is strongly affected by solute diffusion, or in other words, the splitting is affected by the rate at which Al solute diffuses to the advancing γ'/γ interface perpendicular to the applied strain. When there is not enough Al content in the front of the γ'/γ interface, the fast growing γ' particle under applied load may obtain a supplement of Al solute from itself, resulting in a decrease of Al content in the central region of the particle. As a result of this redistribution of Al solute, the γ' particle changed to an alternating γ'–γ lamina as Figs 3(b) and (c) illustrate, which eventually transformed to a doublet of two parallel γ' plates. One may expect that the formation of this transitive γ'–γ lamina is dependent on the splitting rate, influenced by the magnitude of the applied strain. As a matter of fact, transitive γ'–γ laminae containing five parallel γ' plates were observed when the applied strain was increased. However, a lower applied strain has a weaker effect on the splitting of γ' particles. For instance, when the applied strain was 25% decreased from that used to induce particle splitting as shown in Fig. 3, the transitive three-plate splitting stage [see Figs 3(b) and (c)] was not observed. Under this lower applied strain, the splitting process was relatively slow and the solute may redistribute timely, thus only resulting in a doublet of two plates. Further decreasing the applied strain, no splitting was observed.

Since the solute diffusion is dependent on the composition, if the Al content in the matrix is low, the tetragonally growing particle could be more difficult to obtain the Al supplement. As a result, the splitting of a γ' particle may occur under an applied strain which cannot induce the γ' splitting in matrices with higher Al concentrations. In order to confirm this expectation, the growth of a γ' particle in a matrix with a lower Al content ($c_m = 0.06$) was examined. It was observed that the γ' splitting occurred in the matrix of $c_m = 0.06$ under the strain which, however, did not induce the splitting of a γ' particle in the matrix of $c_m = 0.08$. In multi-domain systems, the stress-induced splitting of γ' precipitates is more obvious in a Ni–Al system with low volume fraction of γ' precipitates (i.e. less Al content) than that with a higher volume fraction. Figures 4 and 5 illustrate the γ' splitting in the matrices with volume fractions, respectively, equal to 30 and 45%, induced by a tensile stress (53 MPa). One may see

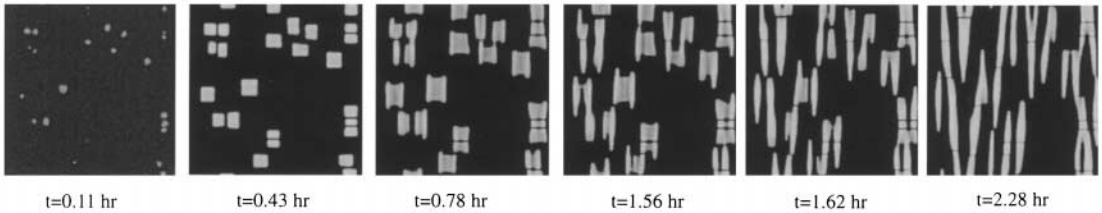

Fig. 4. Splitting of γ' precipitates under a tensile stress (53 MPa) applied vertically. The volume fraction of γ' precipitates is 30%.

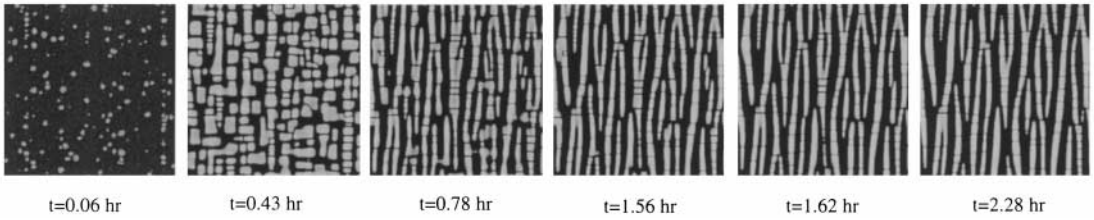

Fig. 5. The splitting of γ' precipitates under the tensile stress (53 MPa) is less obvious when the volume fraction of γ' precipitates is increased to 45%.

that the γ' splitting is more obvious when the volume fraction is lower.

The redistribution of Al solute may also be seen from the variation in composition profile of the γ' precipitate during its growth process. Figures 7(c) and (d) present the composition profiles, corresponding to the doublet illustrated in Fig. 6(d), measured, respectively, along the x- and y-axes across the center of the system. In order to reach the equilibrium state, the total "aging" time was increased from 1.62 to 6.6 h and a smaller system (128×128) was used to save the total computing time. One may see that between the two plates of the doublet, the composition is lower than that of the matrix. It is obvious that the splitting and the growth of the doublet was realized by the redistribution of Al solute through diffusion. For a comparison, the equilibrium composition profile in the stress-free state [Fig. 7(a)] and that under the influence of lattice misfit [Fig. 7(b)] are also illustrated. One may see that the lattice mismatch (i.e. the transformation strain) as well as the external constraint strain change the equilibrium composition profile and result in inhomogeneous composition distributions inside and outside the γ' region.

Effects of compressive applied strains on the splitting of the γ' phase were also investigated. It was observed that the splitting of a γ' particle under an applied compressive strain is similar to that under a tensile strain. However, the splitting under a compressive strain is perpendicular to the applied strain, while the splitting under a tensile strain is along the applied strain.

In summary, the stress-induced splitting results from the stress relaxation and it is also diffusion-dependent.

3.4. Effects of the interfacial energy on the splitting of the γ' phase

It is known that the morphology of a coherent second-phase particle is determined by the competition between the elastic strain energy and the interfacial energy. From the point of view of energy, the splitting of a γ' precipitate increases the interphase boundary area and thus increases the total interfacial energy. As a result of the increase in interfacial energy, the splitting of a γ' precipitate is not favorable. The higher the interfacial energy, the more difficult the splitting. In order to investigate the interfacial effect on the splitting behavior, different values were assigned to the gradient coefficients, α and β, which vary the interfacial energy contribution. In fact, the morphology and splitting are determined by the balance between the interfacial energy and the elastic energy. It is more adequate to use the ratio of the interfacial energy to the elastic energy as a factor to evaluate the effect of interfacial energy. The interfacial energy is the excess free energy associated with the interface, which can be calculated using the following equation:

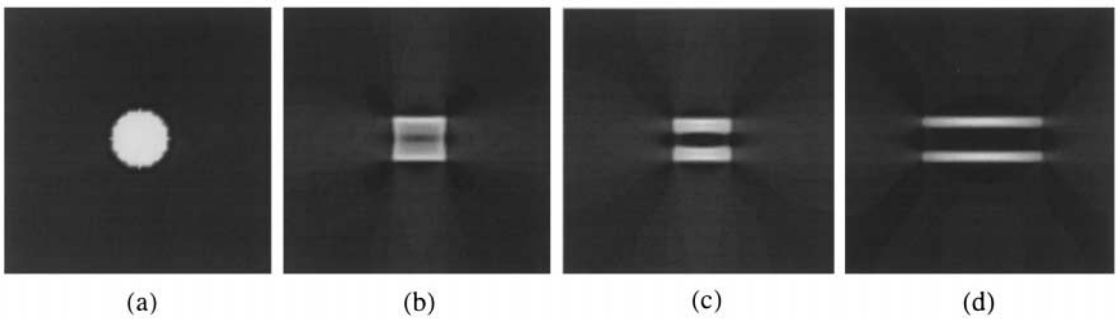

Fig. 6. Splitting of a γ' particle in a γ matrix with $c_m = 0.06$ under a tensile stress $\sigma = 60$ MPa applied along the horizontal direction: (a) $t = 0$; (b) $t = 0.18$ h; (c) $t = 0.54$ h; (d) $t = 1.62$ h.

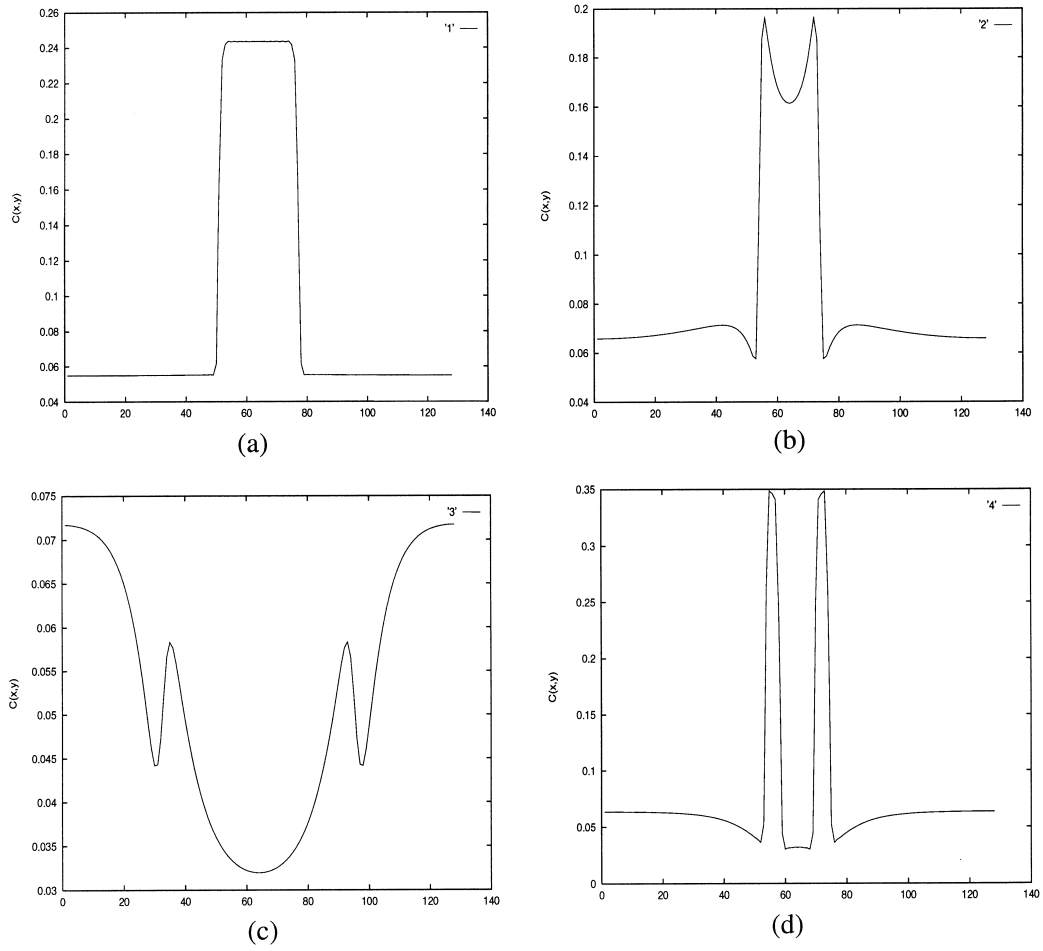

Fig. 7. Equilibrium composition profiles under different constraint conditions, measured along the line across the center of the system: (a) in stress-free condition; (b) under influence of the coherent strain from the lattice mismatch; (c) under a tensile stress initially applied in the horizontal direction, measured along the γ' doublet (i.e. parallel to the applied stress); (d) under the same stress, measured across the γ' doublet.

$$\sigma_{\text{tot}} = \int_V \left[f(C,\eta) - f_0(C) + \frac{3\alpha}{2}(\nabla\eta)^2 + \frac{\beta}{2}(\nabla C)^2 \right] \mathrm{d}^3\vec{r} \tag{14}$$

where

$$f_0(C) = f_{\gamma'}(C_{\gamma'},\eta_0(C_{\gamma'})) + \frac{f_{\gamma'}(C_{\gamma'},\eta_0(C_{\gamma'})) - f_{\gamma}(C_{\text{m}},\eta=0)}{C_{\gamma'} - C_{\text{m}}}(C_0 - C_{\gamma'}). \tag{15}$$

In equation (15), $C_{\gamma'}$ and C_{m} are compositions of the γ' precipitate and the matrix, respectively, and C_0 is the average composition of the system.

Different values of α and β were chosen to investigate the interfacial effect on γ' splitting. Figure 8 illustrates the variation in the splitting behavior of a γ' particle with different ratios of the interfacial energy to the elastic energy, resulting from the variation of α and β coefficients. The corresponding values of the ratio, $\xi = \sigma_{\text{tot}}/E^{\varepsilon}_{\text{el}}$, were calculated. It was demonstrated that the splitting is easier when the ξ value was low; whereas the splitting became difficult as the ξ value increased and even did not occur when the ξ value was high. The simulation demonstrates that the interfacial energy apparently plays an important role in the splitting of the γ' phase. Lee [13] also demonstrated that when the specific interfacial energy is decreased and the coherency strain becomes predominant, the splitting or branching of a coherent precipitate is enhanced.

4. CONCLUSIONS

The morphological evolution and the splitting phenomenon of the γ' phase in γ (NiAl) matrices under applied stresses in the strain constraint condition were studied using a diffuse-interface phase-field simulation approach. The simulation demonstrates that a γ' precipitate exhibits a cuboidal shape with $\{100\}_{\gamma'} \| \{100\}_{\gamma}$, induced mainly by the coherency strain energy. The cuboidal shape can

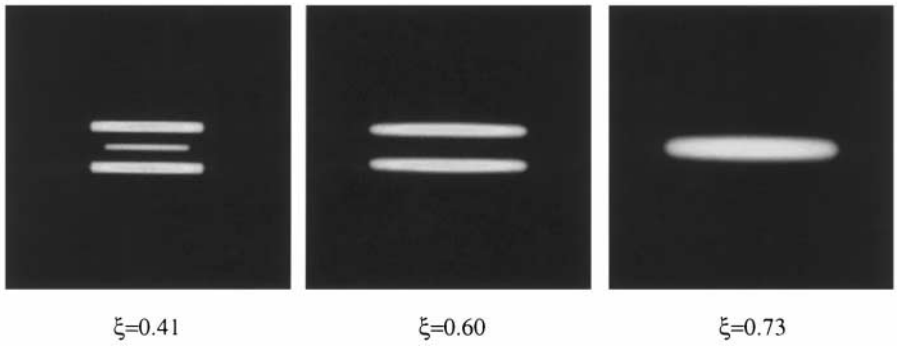

Fig. 8. The splitting of a γ' precipitate is affected by the ratio of the interfacial energy to the elastic energy. $t = 3.24$ h.

change to a tetragonal shape under an applied constraint strain. Under a high applied strain, a γ' precipitate may split into two or more parallel plates during its growth or relaxation to equilibrium. This splitting is favored when the volume fraction of γ' precipitates is low. It was demonstrated that the splitting is also affected by the interfacial energy and the splitting becomes difficult when the ratio of the interfacial energy to the elastic energy is increased.

Acknowledgements—This work was supported by the Office of Naval Research Young Investigator Program under grant number N-00014-95-1-0577 and the simulation was performed at The Pittsburgh Supercomputing Center.

REFERENCES

1. Khachaturyan, A. G., *Theory of Structural Transformations in Solids*. John Wiley, New York, 1983.
2. Johnson, W. C. and Cahn, J. W., *Acta metall.*, 1984, **32**, 1925.
3. Johnson, W. C. and Voorhees, P. W., *J. appl. Phys.*, 1987, **61**, 1610.
4. Khachaturyan, A. G., Semenovskaya, S. V. and Morris, J. W., *Acta metall.*, 1988, **36**, 1563.
5. Miyazaki, T. and Doi, M., *Mater. Sci. Engng*, 1989, **A110**, 175.
6. Wang, Y., Chen, L. Q. and Khachaturyan, A. G., *Scripta metall. mater.*, 1991, **25**, 1387.
7. McCormack, M., Khachaturyan, A. G. and Morris, J. W. Jr, *Acta metall. mater.*, 1992, **40**, 325.
8. Voorhees, P. W., McFadden, G. B. and Johnson, W. C., *Acta metall.*, 1992, **40**, 2979.
9. Nishimori, H. and Onuki, A., *Phys. Lett.*, 1992, **A162**, 323.
10. Thompson, M. E., Su, C. S. and Voorhees, P. W., *J. appl. Phys.*, 1987, **61**, 1610.
11. Wang, Y., Wang, H. Y., Chen, L. Q. and Khachaturyan, A. G., *J. Am. Ceram. Soc.*, 1995, **78**, 657.
12. Lee, J., *Scripta metall.*, 1995, **32**, 559.
13. Lee, J., *Metall. Mater. Trans.*, 1996, **27A**, 1449.
14. Thompson, M. E. and Voorhees, P. W., in *Mathematics of Microstructure Evolution*, ed. L. Q. Chen *et al.* Published jointly by TMS and SLAM, Philadelphia, PA, U.S.A. 1996, p. 125.
15. Jou, H. J., Leo, P. H. and Lowengrub, J. S., *J. Comp. Phys.*, 1997, **131**, 109.
16. Li, D. Y. and Chen, L. Q., *Acta mater.*, 1997, **45**, 2435.
17. Westbrook, J. H., *Z. Kristallogr.*, 1958, **110**, 21.
18. Miyazaki, T., Imamura, H. and Kozakai, T., *Mater. Sci. Engng*, 1982, **54**, 9.
19. Doi, M., Miyazaki, T. and Wakatsuki, T., *Mater. Sci. Engng*, 1984, **67**, 247.
20. Kaufman, M. J., Voorhees, P. W., Johnson, W. C. and Biancaniello, F. S., *Metall. Trans.*, 1989, **20A**, 2171.
21. Yoo, Y. S., Yoon, D. Y. and Henry, M. F., *Metals Mater.*, 1995, **1**, 47.
22. Qu, Y. Y., Calderon, H. A. and Kostorz, G., in *Solid → Solid Phase Transformations*, ed. W. C. Johnson *et al.* Minerals, Metals and Materials Society/ AIME, Warrendale, PA, U.S.A. 1994, p. 599.
23. Zhang, J. D., Li, D. Y. and Chen, L. Q., *Proc. of MRS Fall Meeting*, 1997, to be published.
24. Li, D. Y. and Chen, L. Q., *Scripta mater.*, 1997, **37**, 1271.
25. Wang, Y., Chen, L. Q. and Chachaturyan, A. G., in *Computer Simulation in Materials Science*, ed. H. O. Kirchner *et al.* Kluwer Academic, Dordrecht, 1996, p. 325.
26. Chen, L. Q. and Wang, Y. Z., *J. Metals*, 1996, **12**, 13.
27. Fan, D. and Chen, L. Q., *J. Am. Ceram. Soc.*, 1995, **78**, 769.
28. Li, D. Y. and Chen, L. Q., in *Computer Aided Design of High Temperature Materials*, ed. A. Pechenik, R. K. Kalia and P. Vashishta. Oxford University Press, Oxford, in press.
29. Lai, Z. W., *Phys. Rev.*, 1990, **B41**, 9239.
30. Eshelby, J. D., *Proc. R. Soc.*, 1957, **A241**, 376.
31. Eshelby, J. D., *Proc. R. Soc.*, 1959, **A252**, 561.
32. Walpole, L. J., *Proc. R. Soc.*, 1967, **A300**, 270.
33. Kinoshita, N. and Mura, T., *Physica status solidi (a)*, 1971, **5**, 759.
34. Asaro, R. J. and Barnett, D. M., *J. Mech. Phys. Solids*, 1975, **23**, 77.
35. Mura, T., Mori, T. and Kato, M., *J. Mech. Phys. Solids*, 1976, **24**, 305.
36. Lee, J. K., Barnett, D. M. and Aaronson, H. I., *Metall. Trans.*, 1977, **8A**, 963.
37. Lee, J. K. and Johnson, W. C., *Physica status solidi (a)*, 1976, **46**, 735.
38. Roitburd, A. L., *Solid St. Phys.*, 1978, **33**, 317.
39. Mori, T., Cheng, P. C., Kato, M. and Mura, T., *Acta metall.*, 1978, **26**, 1435.
40. Khachaturyan, A. G., *Soviet Phys.–Solid St.*, 1967, **8**, 2163.
41. Khachaturyan, A. G. and Shatalov, G. A., *Soviet Phys. JETP*, 1969, **29**, 557.
42. Khachaturyan, A. G., Semenovskaya, S. and Tsakalakos, T., *Phys. Rev.*, 1995, **B52**, 1.
43. Allen, S. M. and Cahn, J. W., *Acta metall.*, 1979, **27**, 1085.

44. Cahn, J. W. and Hilliard, J. E., *J. chem. Phys.*, 1958, **28**, 258.
45. Hirata, T. and Kirkwood, D. H., *Acta metall.*, 1977, **25**, 1425.
46. Sequeira, A. D., Calderon, H. A. and Kostorz, G., *Scripta metall. mater.*, 1994, **30**, 7.
47. Pineau, A., *Acta metall.*, 1976, **24**, 559.
48. Tien, J. K. and Copley, S. M., *Metall. Trans.*, 1971, **2**, 543.
49. Miyazaki, T., Nakamura, K. and Mori, H., *J. Mater. Sci.*, 1979, **14**, 1827.
50. Thompson, M. E., Su, C. S. and Voorhees, P. W., *Acta metall. mater.*, 1994, **42**, 2107.
51. Chang, J. C. and Allen, S. M., *J. Mater. Res.*, 1991, **6**, 1843.
52. Wang, Y. and Khachaturyan, A. G., *Acta metall. mater.*, 1995, **43**, 1837.
53. Fredholm, A. and Strudel, J. L., in *Superalloys 1984*, ed. M. Gell, C. S. Kortovich, R. H. Bricknell, W. B. Kent and T. F. Radavich. TMS-MME, Warrendale, Pennsylvania, 1984, p. 211.
54. MacKey, R. A. and Ebert, L. J., *Metall. Trans.*, 1985, **16A**, 1969.
55. Ohe, J. and Wakita, S., in *Superalloys 1984*, ed. M. Gell, C. S. Kortovich, R. H. Bricknell, W. B. Kent and T. F. Radavich. TMS-AIME, Warrendale, Pennsylvania, 1984, p. 93.
56. Laberge, C. A., Fratzl, P. and Lebowitz, J. L., *Acta mater.*, 1997, **45**, 3949.
57. Gayda, J. and Srolovitz, D. J., *Acta mater.*, 1989, **37**, 641.
58. Valles, J. L. and Arrell, D. J., *Acta metall. mater.*, 1994, **42**, 2999.
59. Nishimori, H. and Onuki, A., *Phys. Rev.*, 1990, **B42**, 980.

APPENDIX A

The local elastic modulus tensor of an anisotropic solid containing coherent heterogeneities such as inclusions of a different phase with different elastic moduli may be represented as

$$\lambda_{ijkl}(\vec{r}) = \bar{\lambda}_{ijkl} + \Delta\lambda_{ijkl}\Delta C(\vec{r}) \tag{A1}$$

where $\bar{\lambda}_{ijkl} = \lambda^*_{ijkl}\overline{C(\vec{r})} + \lambda_{ijkl}(1 - \overline{C(\vec{r})})$ is the average elastic modulus. $\Delta\lambda_{ijkl} = \lambda +^*_{ijkl} -\lambda_{ijkl}$ where λ^*_{ijkl} and λ_{ijkl} are, respectively, the elastic moduli of the γ' phase and the matrix. $\Delta C(\vec{r}) = C(\vec{r}) - \bar{C}$.

The elastic strain is the difference between the total strain and the stress-free strain (the matrix is the reference lattice), that is

$$\varepsilon^{\mathrm{el}}_{ij}(\vec{r}) = \varepsilon_{ij}(\vec{r}) - \overset{\circ}{\varepsilon}_{ij}(\vec{r}) = [\bar{\varepsilon}_{ij} + \delta\varepsilon_{ij}(\vec{r})] - \overset{\circ}{\varepsilon}_{ij}(\vec{r}) \tag{A2}$$

where the total strain is expressed as a sum of the homogeneous strain, $\bar{\varepsilon}_{ij}$, and the hetreogeneous strain, $\delta\varepsilon_{ij}(\vec{r})$. The homogeneous strain is the uniform macroscopic strain determining the macroscopic shape deformation of the crystal as a whole produced by both the internal stress due to the presence of new phase particles and the applied strain when the system is under external constraint, i.e. $\bar{\varepsilon}_{ij} = \overset{\circ}{\bar{\varepsilon}}_{ij} + \bar{\varepsilon}^{\mathrm{a}}_{ij}$, where $\overset{\circ}{\bar{\varepsilon}}_{ij}$ is caused by the internal stress and $\bar{\varepsilon}^{\mathrm{a}}_{ij}$ caused by the applied stress. The homogeneous strain is defined such that

$$\int_V \delta\varepsilon_{ij}(\vec{r})\,\mathrm{d}^3\vec{r} = 0 \tag{A3}$$

The stress-free strain, $\overset{\circ}{\varepsilon}_{ij}(\vec{r})$, may be expressed as a function of the composition heterogeneity, i.e. $\overset{\circ}{\varepsilon}_{ij}(\vec{r}) = \overset{\circ}{\varepsilon}_{ij}\Delta C(\vec{r})$, where $\overset{\circ}{\varepsilon}_{ij}$ is the eigenstrain tensor or the transformation strain tensor. It should be pointed out that usually we need structural order parameters to distinguish differently oriented variants of a second phase. However, since in the present case the γ' phase has a pure dilatational mismatch with the matrix, there is no orientational difference between different γ' domains in terms of coherency strain. The stress-free strain can therefore be expressed as a function of the composition heterogeneity only. The elastic stress field is thus given as

$$\sigma_{ij}(\vec{r}) = \lambda_{ijkl}(\vec{r})\varepsilon^{\mathrm{el}}_{kl}(\vec{r}) = [\bar{\lambda}_{ijkl} + \Delta\lambda_{ijkl}\Delta C(\vec{r})][\bar{\varepsilon}_{ij} + \delta\varepsilon_{ij}(\vec{r}) - \overset{\circ}{\varepsilon}_{ij}\Delta C(\vec{r})] \tag{A4}$$

The equilibrium condition

$$\frac{\partial\sigma_{ij}(\vec{r})}{\partial r_j} = 0 \tag{A5}$$

gives

$$\frac{\partial}{\partial r_j}[\bar{\lambda}_{ijkl}\delta\varepsilon_{kl}(\vec{r})] + \frac{\partial}{\partial r_j}[\Delta\lambda_{ijkl}\Delta C(\vec{r})\delta\varepsilon_{kl}(\vec{r})] = [\bar{\lambda}_{ijkl}\overset{\circ}{\varepsilon}_{kl} + 2\Delta\lambda_{ijkl}\overset{\circ}{\varepsilon}_{kl}\Delta C(\vec{r}) - \Delta\lambda_{ijkl}\bar{\varepsilon}_{kl}]\frac{\partial\Delta C(\vec{r})}{\partial r_j} \tag{A6}$$

Khachaturyan *et al.* [42] discussed in detail how to solve the equation which is similar to equation (A6) using the perturbation method where the elastic constant difference $\Delta\lambda_{ijkl}$ plays the role of a small parameter. We used the zeroth approximation by ignoring the second term on the left-hand side of equation (A6) and also the second term in brackets on the right-hand side of equation (A6). It should be noticed that the third term in brackets on the right-hand side of equation (A6) may not be small compared to the first term in the brackets, since the homogeneous strain could be much larger than the transformation strain when the applied strain is large. Therefore, the third term in brackets on the right-hand side can be ignored. Incorporating

$$\delta\varepsilon_{kl}(\vec{r}) = \frac{1}{2}\left(\frac{\partial u_k}{\partial r_l} + \frac{\partial u_l}{\partial r_k}\right)$$

and using the zeroth approximation, we may rewrite equation (A6) as

$$\bar{\lambda}_{ijkl}\frac{\partial^2 u_k}{\partial r_j\partial r_l} = [\bar{\lambda}_{ijkl}\overset{\circ}{\varepsilon}_{kl} - \Delta\lambda_{ijkl}\bar{\varepsilon}_{kl}]\frac{\partial\Delta C(\vec{r})}{\partial r_j} = \sigma^*_{ij}\frac{\partial\Delta C(\vec{r})}{\partial r_j} \tag{A7}$$

where $\sigma^*_{ij} = \bar{\lambda}_{ijkl}\overset{\circ}{\varepsilon}_{kl} - \Delta\lambda_{ijkl}\bar{\varepsilon}_{kl}$ is the effective eigenstress. Fourier transforming equation (A7) into reciprocal space, we may obtain

$$\bar{\lambda}_{ijkl}q_jq_lv_k(\vec{q}) = -\mathrm{i}\sigma^*_{ij}q_j\Delta C(\vec{q}) \tag{A8}$$

where

$$v_k(\vec{q}) = \int_V u_k(\vec{r})\,\mathrm{e}^{-\mathrm{i}\vec{q}\cdot\vec{r}}\,\mathrm{d}^3\vec{r},\quad \tilde{C}(\vec{q}) = \int_V \Delta C(\vec{r})\,\mathrm{e}^{-\mathrm{i}\vec{q}\cdot\vec{r}}\,\mathrm{d}^3\vec{r}.$$

If $q \neq 0$, we have

$$v_k(\vec{q}) = -\mathrm{i}G_{ik}(\vec{q})\sigma^*_{ij}q_j\tilde{C}(\vec{q})$$

where the matrix $G_{ik}(\vec{q})$, the reverse tensor to $(G^{-1}(\vec{q}))_{ik} = \bar{\lambda}_{ijkl}q_jq_l$, is the Fourier transform of the Green function of anisotropic elasticity; by definition, $(G^{-1}(\vec{q}))_{ik} = q^2\bar{\lambda}_{ijkl}n_jn_l$, where $\vec{n} = \vec{q}/q$ is a unit reciprocal lattice vector. The singular branching point $k = 0$ is excluded. The Green function $G_{ik}(\vec{q})$ can therefore be rewritten in the form $G_{ik}(\vec{q}) = (1/q^2)\Omega_{ik}(\vec{n})$, where $\Omega^{-1}_{ik}(\vec{q}) = \bar{\lambda}_{ijkl}n_jn_l$. The total elastic energy of a coherent mixture is represented as

$$E_{\mathrm{el}} = \frac{1}{2}\int_V [\bar{\lambda}_{ijkl} + \Delta\lambda_{ijkl}\Delta C(\vec{r})][\bar{\varepsilon}_{kl} + \delta\varepsilon_{kl}(\vec{r}) - \overset{\circ}{\varepsilon}_{kl}\Delta C(\vec{r})]$$
$$\times [\bar{\varepsilon}_{ij} + \delta\varepsilon_{ij}(\vec{r}) - \overset{\circ}{\varepsilon}_{ij}\Delta C(\vec{r})]\,\mathrm{d}^3\vec{r} \approx \frac{V}{2}\bar{\lambda}_{ijkl}\bar{\varepsilon}_{ij}\bar{\varepsilon}_{kl}$$
$$- V\Delta\lambda_{ijkl}\bar{\varepsilon}_{ij}\overset{\circ}{\varepsilon}_{kl}\overline{(\Delta C)^2} + \frac{V}{2}\bar{\lambda}_{ijkl}\overset{\circ}{\varepsilon}_{kl}\overset{\circ}{\varepsilon}_{ij}\overline{(\Delta C)^2}$$
$$+ \frac{1}{2}\int_V \bar{\lambda}_{ijkl}\delta\varepsilon_{ij}(\vec{r})\delta\varepsilon_{kl}(\vec{r})\,\mathrm{d}^3\vec{r} - \int_V \sigma^*_{ij}\delta\varepsilon_{ij}\Delta C(\vec{r})\,\mathrm{d}^3\vec{r}$$
$$= \frac{V}{2}\bar{\lambda}_{ijkl}\bar{\varepsilon}_{ij}\bar{\varepsilon}_{kl} - V\Delta\lambda_{ijkl}\bar{\varepsilon}_{ij}\overset{\circ}{\varepsilon}_{kl}\overline{(\Delta C)^2} + \frac{V}{2}\bar{\lambda}_{ijkl}\overset{\circ}{\varepsilon}_{kl}\overset{\circ}{\varepsilon}_{ij}\overline{(\Delta C)^2}$$
$$+ \frac{1}{2}\int_V \left[\bar{\lambda}_{ijkl}\frac{\partial u_i}{\partial r_j}\frac{\partial u_k}{\partial r_l} - \sigma^*_{ij}\frac{\partial u_i}{\partial r_j}\Delta C(\vec{r})\right]\mathrm{d}^3\vec{r}. \quad \text{(A9)}$$

In the above derivation, the zeroth approximation was used. Substituting the back Fourier transforms

$$\vec{u}(\vec{r}) = \int \frac{\mathrm{d}^3\vec{q}}{(2\pi)^3}\vec{v}(\vec{q})\,\mathrm{e}^{\mathrm{i}\vec{q}\cdot\vec{r}},\ \Delta C(\vec{r}) = \int \frac{\mathrm{d}^3\vec{q}}{(2\pi)^3}\tilde{C}(\vec{q})\,\mathrm{e}^{\mathrm{i}\vec{q}\cdot\vec{r}}$$

into equation (A9), integrating equation (A9) over $\vec{r}$ and applying the relation

$$\int_V \mathrm{e}^{\mathrm{i}(\vec{q}+\vec{q}')\cdot\vec{r}}\,\mathrm{d}^3\vec{r} = (2\pi)^3\delta(\vec{q}+\vec{q}') \quad \text{(A10)}$$

where $\delta(\ldots)$ is the Dirac delta function, we may obtain

$$E_{\mathrm{el}} = \frac{V}{2}\bar{\lambda}_{ijkl}\bar{\varepsilon}_{ij}\bar{\varepsilon}_{kl} - V\Delta\lambda_{ijkl}\bar{\varepsilon}_{ij}\overset{\circ}{\varepsilon}_{kl}\overline{(\Delta C)^2} + \frac{V}{2}\bar{\lambda}_{ijkl}\overset{\circ}{\varepsilon}_{ij}\overset{\circ}{\varepsilon}_{kl}\overline{(\Delta C)^2}$$
$$+ \int \frac{\mathrm{d}^3\vec{q}}{(2\pi)^3}\left[\frac{1}{2}\bar{\lambda}_{ijkl}q_jq_lv_i(\vec{q})v_k^*(\vec{q}) - \mathrm{i}\sigma^*_{ij}q_jv_i(\vec{q})\tilde{C}^*(\vec{q})\right] \quad \text{(A11)}$$

Substituting the solution for $v_i(\vec{q})$, we obtain the final expression of the total elastic energy

$$E_{\mathrm{el}} = \frac{V}{2}\bar{\lambda}_{ijkl}\bar{\varepsilon}_{ij}\bar{\varepsilon}_{kl} - V\Delta\lambda_{ijkl}\bar{\varepsilon}_{ij}\overset{\circ}{\varepsilon}_{kl}\overline{(\Delta C)^2} + \frac{V}{2}\bar{\lambda}_{ijkl}\overset{\circ}{\varepsilon}_{ij}\overset{\circ}{\varepsilon}_{kl}\overline{(\Delta C)^2}$$
$$- \frac{1}{2}\int \frac{\mathrm{d}^3\vec{q}}{(2\pi)^3}[\vec{n}\sigma^*\Omega(\vec{n})\sigma^*\vec{n}]|\tilde{C}(\vec{q})|^2. \quad \text{(A12)}$$

The formula of the elastic energy may change under different boundary conditions.

Fixed boundary

If the boundary of the system is fixed and hence no homogeneous strain is allowed, the elastic energy is given by

$$E_{\mathrm{el}} = \frac{V}{2}\bar{\lambda}_{ijkl}\overset{\circ}{\varepsilon}_{ij}\overset{\circ}{\varepsilon}_{kl}\overline{(\Delta C)^2} - \frac{1}{2}\int \frac{\mathrm{d}^3\vec{q}}{(2\pi)^3}[\vec{n}\sigma^*\Omega(\vec{n})\sigma^*\vec{n}]|\tilde{C}(\vec{q})|^2 \quad \text{(A13)}$$

where

$$\sigma^*_{ij} = \bar{\lambda}_{ijkl}\overset{\circ}{\varepsilon}_{kl}$$

Constant homogeneous applied strain—strain constraint

In this case, the system is initially strained, followed by fixing the boundary. The elastic energy becomes

$$E^{\varepsilon}_{\mathrm{el}} = \frac{V}{2}\bar{\lambda}_{ijkl}\bar{\varepsilon}^{\mathrm{a}}_{ij}\bar{\varepsilon}^{\mathrm{a}}_{kl} - V\Delta\bar{\lambda}_{ijkl}\bar{\varepsilon}^{\mathrm{a}}_{ij}\overset{\circ}{\varepsilon}_{kl}\overline{(\Delta C)^2} + \frac{V}{2}\bar{\lambda}_{ijkl}\overset{\circ}{\varepsilon}_{ij}\overset{\circ}{\varepsilon}_{kl}\overline{(\Delta C)^2}$$
$$- \frac{1}{2}\int \frac{\mathrm{d}^3\vec{q}}{(2\pi)^3}[\vec{n}\sigma^*\Omega(\vec{n})\sigma^*\vec{n}]|\tilde{C}(\vec{q})|^2 \quad \text{(A14)}$$

where the effective eigenstress is given by

$$\sigma^*_{ij} = \bar{\lambda}_{ijkl}\overset{\circ}{\varepsilon}_{kl} - \Delta\lambda_{ijkl}\bar{\varepsilon}^{\mathrm{a}}_{kl}.$$

Stress-free boundary

When the boundary of a system is free to relax, the homogeneous strain is obtained by minimizing the total elastic energy given by equation (A12)

$$\frac{\partial E}{\partial\bar{\varepsilon}_{ij}} = 0 = V\bar{\lambda}_{ijkl}\bar{\varepsilon}_{kl} - V\Delta\lambda_{ijkl}\overset{\circ}{\varepsilon}_{kl}\overline{(\Delta C)^2}$$
$$+ \Delta\lambda_{ijkl}A_{klmn}(\bar{\lambda}_{mnop}\overset{\circ}{\varepsilon}_{op} - \Delta\lambda_{mnop}\bar{\varepsilon}_{op}) \quad \text{(A15)}$$

where

$$A_{klmn} = -\int \frac{\mathrm{d}^3\vec{q}}{(2\pi)^3}n_k\Omega_{lm}n_n|\tilde{C}(\vec{q})|^2. \quad \text{(A16)}$$

From equation (A15), the homogeneous strain may be represented as

$$(V\bar{\lambda}_{ijop} - \Delta\lambda_{ijkl}A_{klmn}\Delta\lambda_{mnop})\bar{\varepsilon}_{op} = V\Delta\lambda_{ijop}\overset{\circ}{\varepsilon}_{op}\overline{(\Delta C)^2}$$
$$- \Delta\lambda_{ijkl}A_{klmn}\bar{\lambda}_{mnop}\overset{\circ}{\varepsilon}_{op}. \quad \text{(A17)}$$

By multiplying both sides of equation (A17) by $\bar{S}_{ijop}$, the average elastic compliance tensor, and using the zeroth approximation with respect to elastic modulus misfit $\Delta\lambda_{ijkl}$, we have

$$\bar{\varepsilon}_{op} \approx \left(\bar{S}_{opij}\Delta\lambda_{ijsq}\overset{\circ}{\varepsilon}_{sq}\overline{(\Delta C)^2} - \frac{\Delta\lambda_{oplm}A_{lmsq}}{V}\right)\overset{\circ}{\varepsilon}_{sq} \quad \text{(A18)}$$

Constant homogeneous applied stress—stress constraint

When a constant stress is applied, the total potential energy is the sum of the elastic energy of the system and the potential energy of the mechanical loading device, that is

$$E^{\sigma}_{\mathrm{el}} = \frac{V}{2}\bar{\lambda}_{ijkl}\bar{\varepsilon}_{ij}\bar{\varepsilon}_{kl} - V\Delta\lambda_{ijkl}\bar{\varepsilon}_{ij}\overset{\circ}{\varepsilon}_{kl}\overline{(\Delta C)^2} + \frac{V}{2}\bar{\lambda}_{ijkl}\overset{\circ}{\varepsilon}_{ij}\overset{\circ}{\varepsilon}_{kl}\overline{(\Delta C)^2}$$
$$- \frac{1}{2}\int \frac{\mathrm{d}^3\vec{q}}{(2\pi)^3}[\vec{n}\sigma^*\Omega(\vec{n})\sigma^*\vec{n}]|\tilde{C}(\vec{q})|^2 - \int_V \sigma^{\mathrm{a}}_{ij}\bar{\varepsilon}_{ij}\,\mathrm{d}^3\vec{r}. \quad \text{(A19)}$$

Minimizing the total potential energy with respect to the homogeneous strain

$$\frac{\partial E}{\partial\bar{\varepsilon}_{ij}} = 0 = V\bar{\lambda}_{ijkl}\bar{\varepsilon}_{kl} - V\Delta\lambda_{ijkl}\overset{\circ}{\varepsilon}_{kl}\overline{(\Delta C)^2}$$
$$+ \Delta\lambda_{ijkl}A_{klmn}(\bar{\lambda}_{mnop}\overset{\circ}{\varepsilon}_{op} - \Delta\lambda_{mnop}\bar{\varepsilon}_{op}) - V\sigma^{\mathrm{a}}_{ij} \quad \text{(A20)}$$

we may obtain

$$\sigma^{\mathrm{a}}_{ij} = \bar{\lambda}_{ijkl}\bar{\varepsilon}_{kl} - \Delta\lambda_{ijkl}\overset{\circ}{\varepsilon}_{kl}\overline{(\Delta C)^2}$$
$$+ \frac{1}{V}\Delta\lambda_{ijkl}A_{klmn}(\bar{\lambda}_{mnop}\overset{\circ}{\varepsilon}_{op} - \Delta\lambda_{mnop}\bar{\varepsilon}_{op}) \quad \text{(A21)}$$

By multiplying both sides of equation (A21) by $\bar{S}_{ijop}$ and using the zeroth approximation with respect to elastic modulus misfit $\Delta\lambda_{ijkl}$, we may approximately express the homogeneous strain as

$$\bar{\varepsilon}_{op} \approx \left(\bar{S}_{opij}\Delta\lambda_{ijsq}\overset{\circ}{\varepsilon}_{sq}\overline{(\Delta C)^2} - \frac{\Delta\lambda_{oplm}A_{lmsq}}{V}\right)\overset{\circ}{\varepsilon}_{sq} + \bar{S}_{opij}\sigma^{\mathrm{a}}_{ij} \quad \text{(A22)}$$